EUROPEAN ORGANIZATION FOR NUCLEAR RESEARCH

Measurement of inclusive and leading subjet fragmentation in pp and Pb–Pb collisions at $\sqrt{s_{\mathrm{NN}}} = 5.02$ TeV

ALICE Collaboration

Abstract

This article presents new measurements of the fragmentation properties of jets in both proton–proton (pp) and heavy-ion collisions with the ALICE experiment at the Large Hadron Collider (LHC). We report distributions of the fraction z_r of transverse momentum carried by subjets of radius r within jets of radius R. Charged-particle jets are reconstructed at midrapidity using the anti-k_{T} algorithm with jet radius $R = 0.4$, and subjets are reconstructed by reclustering the jet constituents using the anti-k_{T} algorithm with radii $r = 0.1$ and $r = 0.2$. In proton–proton collisions, we measure both the inclusive and leading subjet distributions. We compare these measurements to perturbative calculations at next-to-leading logarithmic accuracy, which suggest a large impact of threshold resummation and hadronization effects on the z_r distribution. In heavy-ion collisions, we measure the leading subjet distributions, which allow access to a region of harder jet fragmentation than has been probed by previous measurements of jet quenching via hadron fragmentation distributions. The z_r distributions enable extraction of the parton-to-subjet fragmentation function and allow for tests of the universality of jet fragmentation functions in the quark–gluon plasma (QGP). We find indications that there is a turnover in the ratio between the distributions in Pb–Pb and pp collisions as $z_r \to 1$, exposing qualitatively new possibilities to disentangle competing jet quenching mechanisms. By comparing our results to theoretical calculations based on an independent extraction of the parton-to-jet fragmentation function, we find consistency with the universality of jet fragmentation and no indication of factorization breaking in the QGP.

1 Introduction

Measurements of high-energy jets produced in scattering experiments offer opportunities to test pertur-bative calculations in quantum chromodynamics (QCD) [1–9] and to probe the properties of the quark–gluon plasma (QGP) [10–15]. Heavy-ion collisions can be used to produce short-lived droplets of QGP, serving as a laboratory system to study the emergence of this high-temperature, strongly-coupled, de-confined system of quarks and gluons in QCD. While several of its transport coefficients have been con-strained by experimental measurements [16–26], the detailed physical properties of the QGP, including the nature of its degrees of freedom as a function of resolution scale, remain unknown.

Properties of the QGP can be inferred by comparing jets in heavy-ion collisions, which traverse the QGP, to their counterparts in proton–proton collisions. Significant experimental and theoretical effort has been made to measure and calculate the modification of jet observables in heavy-ion collisions, known as jet quenching, in an ongoing attempt to achieve a unified description of the jet–QGP interaction [27–29]. It has been established that jets traversing the QGP emit soft medium-induced radiation outside of the jet cone, causing their observed yields to be significantly suppressed as compared to pp collisions, and that the fragmentation pattern of the resulting observed jets can be both narrowed and hardened in certain regions of phase space [30–43]. However, the precise role of several theoretical mechanisms of jet quenching, such as quark vs. gluon energy loss, factorization breaking, and color coherence remains unclear. It is essential to understand and disentangle these mechanisms in order to use jet quenching to reveal physical properties of the QGP.

In this article, we consider measurements of charged-particle *subjets*, defined by first clustering inclusive charged-particle jets with the anti-k_T algorithm [44] with radius R, and then reclustering the jet con-stituents with the anti-k_T algorithm with subjet radius $r < R$, as illustrated in Fig. 1 [45]. We focus on the fraction of charged-particle transverse momentum (p_T) carried by the subjet:

$$z_r = \frac{p_T^{\text{ch subjet}}}{p_T^{\text{ch jet}}},$$

where $p_T^{\text{ch (sub)jet}}$ is the transverse momentum of the charged-particle (sub)jet.

In pp collisions, both the inclusive and leading subjet z_r distributions have been calculated perturbatively for a variety of r and R values [46, 47]. These calculations involve several interesting aspects that can be studied experimentally such as the role of threshold resummation, and, in the leading subjet case, nonlinear evolution of the jet fragmentation function. Similar effects have recently been examined in e^+e^- collisions [8, 47].

In heavy-ion collisions, subjet observables have been proposed as sensitive probes of jet quenching [46–49]. The subjet z_r observable presents several unique opportunities to study jet quenching:

1. *Probe high-z fragmentation.* The subjet fragmentation distribution z_r is complementary to the lon-gitudinal momentum fraction z of hadrons in jets [36–39]. The subjet fragmentation distribution can be understood as a generalization of the hadron fragmentation distribution, where in the limit $r \to 0$ the two become equal. Subjet measurements offer the benefit of probing higher z values than hadron measurements, enabling a more precise handle on the overall hardness of jet fragmentation, and thereby make it possible to access a quark-dominated sample of jets [47]. This in turn provides an opportunity to expose the interplay of soft medium-induced radiation with the relative suppres-sion of gluon vs. quark jets, and introduces a method to do so based on inclusive jet samples alone, complementary to existing methods comparing inclusive and photon-tagged jet observables [37,39].

2. *Test the universality of jet fragmentation in the QGP.* In vacuum, it is expected that the parton-to-jet fragmentation function, $J(z)$, is equal to the parton-to-subjet fragmentation function $J_r(z)$ [46]. However, it is unknown whether this universality of jet fragmentation functions holds in the QGP
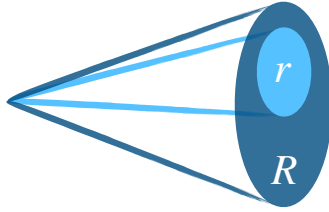
Figure 1: Cartoon of a subjet of radius r inside a jet of radius R. We consider charged-particle subjets clustered using the anti-k_T algorithm from the constituents of inclusive charged-particle jets.

independently of the observable considered [50]. Measurements of z_r distributions are directly sensitive to the medium-modified parton-to-subjet fragmentation function, $J_{r,\mathrm{med}}(z)$, and can be used to extract it. The extracted $J_{r,\mathrm{med}}(z)$ can then be compared to an independently extracted medium-modified parton-to-jet fragmentation function, $J_{\mathrm{med}}(z)$, to test the universality of in-medium jet fragmentation across different jet observables in heavy-ion collisions and look for signs of factorization breaking.

3. *Measure energy loss at the cross section level.* A well-defined method of measuring out-of-cone energy loss at the cross section level has been proposed by computing moments of the leading subjet z_r distribution [47]. The first moment or "subjet energy loss" describes the fraction of jet p_T not carried by the leading subjet, and higher moments describe fluctuations in this energy loss. These quantities can be computed in both pp and Pb–Pb collisions for a variety of r and R values, and contrasted with other measures of jet modification.

2   Experimental setup and data sets

A description of the ALICE detector and its performance can be found in Refs. [51, 52]. The data sample of pp collisions used in this analysis was collected in 2017 during the LHC Run 2 at $\sqrt{s} = 5.02$ TeV using a minimum-bias (MB) trigger defined by the coincidence of the signals from the two V0 scintillator arrays in the forward region [53]. The Pb–Pb data set was collected in 2018 at $\sqrt{s_{\mathrm{NN}}} = 5.02$ TeV. A central collision trigger was used which selects events in the 0–10% centrality interval based on the multiplicity of produced particles in the V0 detector acceptance [54, 55]. In the event, the primary vertex was required to be within 10 cm along the beam axis from the center of the detector. Beam-induced background events were removed using timing information from the V0 detectors and, in Pb–Pb collisions, from two neutron Zero Degree Calorimeters located ± 112.5 m along the beam axis from the center of the detector. Pileup events were rejected based on multiple reconstructed vertices and tracking selections [30]. After these selections, the pp data sample contains 870 million events and corresponds to an integrated luminosity of 18.0 ± 0.4 nb^{-1} [56]. The Pb–Pb data sample contains 92 million events in 0–10% central collisions, corresponding to an integrated luminosity of approximately 0.12 nb^{-1}.

This analysis uses charged-particle tracks reconstructed based on the information from the Time Projection Chamber (TPC) [57] and the Inner Tracking System (ITS) [58]. While track-based observables are collinear-unsafe [59–61], they can be measured with greater precision than calorimeter-based observables, and recent measurements have demonstrated that for many substructure observables track-based distributions are compatible with the corresponding collinear-safe distributions [4]. We define two types of tracks: global tracks and complementary tracks [52]. Global tracks are required to include at least one hit in the Silicon Pixel Detector (SPD) comprising the two innermost layers of the ITS and to satisfy multiple criteria on the quality of track reconstruction in the TPC and its pointing to the collision vertex. Complementary tracks are all those satisfying all the selection criteria of global tracks except for the request of a point in the SPD. They are refitted using the primary vertex to constrain their trajectory in order to preserve good momentum resolution, especially at high transverse momentum (p_T). Including this

second class of tracks ensures approximately uniform azimuthal acceptance, while providing similar p_T resolution to tracks with SPD hits. Tracks with $p_T > 0.15\,\text{GeV}/c$ were accepted over the pseudorapidity range $|\eta| < 0.9$ and azimuthal angle $0 < \varphi < 2\pi$. The momentum resolution $\sigma(p_T)/p_T$ of the accepted tracks was estimated from the covariance matrix of the track fit parameters [52], and is approximately 1% at track $p_T = 1\,\text{GeV}/c$ and 4% at $p_T = 50\,\text{GeV}/c$.

The instrumental performance of the detector was estimated with a simulation performed using PYTHIA8 Monash 2013 [62, 63] for the event generation and the GEANT3 transport code [64] to propagate particles through the simulated ALICE apparatus. The tracking efficiency in pp collisions is approximately 67% at track $p_T = 0.15\,\text{GeV}/c$, and rises to approximately 84% at $p_T = 1\,\text{GeV}/c$, and remains above 75% at higher p_T. Studies of the centrality dependence of the tracking efficiency in a HIJING [65] simulation demonstrated that the tracking efficiency is approximately 2% lower in 0–10% central Pb–Pb collisions compared to pp collisions, independent of track p_T.

3   Analysis method

Jets were reconstructed from charged-particle tracks with FastJet 3.2.1 [66] using the anti-k_T algorithm with E-scheme recombination and radius (or resolution parameter) $R = 0.4$ [44, 67]. Subjets were reconstructed by reclustering the jet constituents using the anti-k_T algorithm with E-scheme recombination and radii $r = 0.1$ and $r = 0.2$. The pion mass was assumed for all jet constituents. Jets containing tracks with $p_T > 100\,\text{GeV}/c$, corresponding to $< 1\%$ of the jet sample in the considered kinematic range, were discarded in order to ensure good momentum determination. Jets in heavy-ion collisions have a large uncorrelated background contribution due to the underlying event (UE) [68]. The event-by-event constituent subtraction method was used before jet finding was performed [69, 70]. This corrects the overall jet p_T and its substructure simultaneously by subtracting UE energy constituent by constituent. A maximum recombination distance $R_{\text{max}} = 0.25$ was used. In pp collisions, the UE was not subtracted. The jet axis is required to be within the fiducial volume of the TPC, $|\eta_{\text{jet}}| < 0.9 - R$, where η_{jet} is the jet axis pseudorapidity.

The jet reconstruction performance is studied by simulating pp events and particle transport through the ALICE detector material as described in Sec. 2. We compare PYTHIA8 generated jets at "truth level" (before the particles undergo interactions with the detector) to those at "detector level" (after detector simulation). The truth-level jet was constructed from the charged primary particles of the PYTHIA8 event, defined as all particles with a mean proper lifetime larger than 1 cm/c, and excluding the decay products of these particles [71]. For the Pb–Pb data analysis, we embedded the simulated pp events after track reconstruction into 0–10% centrality Pb–Pb measured events to account for background effects, and applied the constituent subtraction procedure described above. A jet matching procedure is used in order to associate jets at the truth level to jets at the detector level. In pp collisions, this matching procedure is based on geometrically matching jets within $\Delta R < 0.6\,R$, where $\Delta R = \sqrt{\Delta y^2 + \Delta \varphi^2}$ is their rapidity-azimuth separation. In Pb–Pb collisions, the matching procedure includes both this geometrical requirement and further requires that the jet contains at least 50% of the total track p_T of the associated reconstructed jet from the embedded pp event at detector level. To study the subjet z_r reconstruction performance, a similar matching procedure was adopted. In order to match inclusive subjets at the truth level with their counterparts at the detector level, we apply the same matching procedure as described above for jets, except with the subjet radius r replacing the jet radius R in the geometrical matching criteria. In the case of leading subjets, however, we match the leading subjet at the truth level to the leading subjet at the detector level, without requiring geometrical criteria. The jet energy scale shift $(p_{T,\text{det}}^{\text{ch jet}} - p_{T,\text{truth}}^{\text{ch jet}})/p_{T,\text{truth}}^{\text{ch jet}}$ is a long-tailed asymmetric distribution due to tracking inefficiency with a peak at zero, corresponding to $p_{T,\text{det}}^{\text{ch jet}} = p_{T,\text{truth}}^{\text{ch jet}}$, where $p_{T,\text{det}}^{\text{ch jet}}$ is the detector-level $p_T^{\text{ch jet}}$, and $p_{T,\text{truth}}^{\text{ch jet}}$ is the truth-level $p_T^{\text{ch jet}}$ [72]. The mean jet energy scale shift for $R = 0.4$ charged-particle jets in pp collisions is

approximately -13% at $p_{\mathrm{T,truth}}^{\mathrm{ch\,jet}} = 20\,\mathrm{GeV}/c$ and decreases to -21% at $p_{\mathrm{T,truth}}^{\mathrm{ch\,jet}} = 100\,\mathrm{GeV}/c$. The jet energy resolution is approximately constant at 21% in pp collisions; in Pb–Pb collisions an additional contribution from the underlying event fluctuations further broadens the distribution of the jet energy scale shift, with the standard deviation of the background fluctuation contribution to the shift $\sigma_{\delta p_{\mathrm{T}}}$ [68] being equal to approximately $11\,\mathrm{GeV}/c$, independent of $p_{\mathrm{T,truth}}^{\mathrm{ch\,jet}}$. The z_r reconstruction performance behaves qualitatively similarly as the jet p_{T} described above, with a peak near zero in the relative residual distribution corresponding to $z_{r,\mathrm{det}} = z_{r,\mathrm{truth}}$. The z_r reconstruction resolution is $\mathcal{O}(10\%)$, with asymmetric tails that are broader for small z_r than for large z_r, and broader in Pb–Pb compared to pp collisions.

Local fluctuations in the underlying event of a heavy-ion collision can result in an incorrect subjet (unrelated to the hard scattering) being identified by the reclustering algorithm. This "mistagging" effect is in exact analogy to the case of identifying groomed jet splittings in the presence of a large underlying event [73], although with improved robustness to mistagging effects [74]. In order to address this issue, the measurement was performed by restricting to $z_{r,\mathrm{det}} > 0.5$, which mitigates these effects. The subjet purity due to these background effects was evaluated by embedding jets simulated with the PYTHIA8 event generator [62] into measured Pb–Pb collisions and following the procedure in Ref. [73] . The residual background contribution remains below 5% for $z_r > 0.6$ and increases up to approximately 20% at $z_r = 0.5$, for the $p_{\mathrm{T,det}}^{\mathrm{ch\,jet}}$ range considered in this measurement. This level of background contamination is small enough to allow the results to be unfolded for detector effects and background fluctuations. The corresponding contamination in pp collisions is negligible.

The reconstructed $p_{\mathrm{T}}^{\mathrm{ch\,jet}}$ and z_r differ from their true values due to tracking inefficiency, particle-material interactions, and track p_{T} resolution. Moreover, in Pb–Pb collisions, background fluctuations significantly smear the reconstructed distributions of z_r. To account for these effects, we simulated events at the truth level and detector level and matched both jets and subjets at the truth level and detector level as described above. We constructed a 4D response matrix (RM) that describes the detector and background response in $p_{\mathrm{T}}^{\mathrm{ch\,jet}}$ and z_r: $R\left(p_{\mathrm{T,det}}^{\mathrm{ch\,jet}}, p_{\mathrm{T,truth}}^{\mathrm{ch\,jet}}, z_{r,\mathrm{det}}, z_{r,\mathrm{truth}}\right)$. A simultaneous unfolding was then performed in $p_{\mathrm{T}}^{\mathrm{ch\,jet}}$ and z_r using the iterative Bayesian unfolding algorithm [75, 76] implemented in the RooUnfold package [77]. In Pb–Pb collisions, lower limits of $p_{\mathrm{T,det}}^{\mathrm{ch\,jet}} > 60\,\mathrm{GeV}/c$ and $z_{r,\mathrm{det}} > 0.5$ are imposed on the data that is input to the unfolding, in order to reject combinatorial jets and mistagged subjets. No such limitation is imposed on $p_{\mathrm{T,truth}}^{\mathrm{ch\,jet}}$ or $z_{r,\mathrm{truth}}$ during the unfolding process. The distributions were corrected for "misses", in which a jet was generated inside the considered truth-level range but not inside the detector-level range. The rate of "fakes", in which a jet exists inside the considered detector-level range but not inside the truth-level range, is $< 1\%$ and therefore negligible. The number of iterations, which sets the strength of regularization, was chosen by minimizing the quadratic sum of the statistical and systematic unfolding uncertainties. This results in the optimal number of iterations equal to 3 in all cases.

To validate the performance of the unfolding procedure, we performed refolding tests, in which the RM is multiplied by the unfolded solution and compared to the original detector-level spectrum. We also did closure tests, in which the shape of the input MC spectrum is modified to account for the possibility that the true distribution may be different from the MC input spectrum (using the same scalings as for the systematic variations in the unfolding prior described below in Sec. 4). In all cases, successful closure was obtained within statistical uncertainties. Additionally, we performed a closure test to quantify the sensitivity of the final result to combinatorial jets and background subjets. This consisted of redoing the entire analysis on "combined" events containing a PYTHIA8 event and a thermal background, in which "combined" jets were clustered from the combination of PYTHIA8 detector-level particles and thermal background particles. The background was modeled by generating N particles with p_{T} taken from a Gamma distribution, $f_{\Gamma}(p_{\mathrm{T}}; \beta) \propto p_{\mathrm{T}} e^{-p_{\mathrm{T}}/\beta}$, where N and β were fixed to roughly fit the $R = 0.4$ δp_{T} distribution in Pb–Pb data [68]. This background model was verified to describe the subjet purity to percent-level accuracy. The test consisted of constructing the combined detector-level jet spectrum,

building the RM, unfolding the combined jets, and comparing the spectrum to the truth-level PYTHIA8 spectrum. Because the background does not contain hard jets, this test is able to quantify the extent to which the analysis procedure recovers the signal distribution and is free of background contamination. The unfolded combined jet spectrum was found to be consistent with the truth-level spectrum within statistical uncertainties, thus confirming a successful closure.

4 Systematic uncertainties

The systematic uncertainties in this measurement are due to the tracking efficiency, the unfolding procedure, the model dependence of the event generator, and in the case of Pb–Pb collisions, the background subtraction procedure. Table 1 summarizes the systematic uncertainty contributions for pp and Pb–Pb collisions for the two considered values of r. The total systematic uncertainty is calculated as the sum in quadrature of all of the individual sources described below.

The systematic uncertainty due to the uncertainty in tracking efficiency is evaluated by randomly discarding charged tracks before jet finding. The tracking efficiency uncertainty, estimated from the variation of the track selection criteria and a detailed study of the ITS–TPC track-matching efficiency uncertainty, is 4%. In order to assign a systematic uncertainty to the final result, we constructed an alternative RM with this random track rejection and repeated the unfolding procedure. The result was compared to the default result, with the differences in each bin taken as the systematic uncertainty. The uncertainty on the track momentum resolution is a sub-leading effect to the tracking efficiency and is negligible.

Several variations of the unfolding procedure are performed in order to estimate the systematic uncertainty arising from the unfolding regularization:

- The number of iterations in the unfolding was varied by ± 2 units and the average difference with respect to the nominal result is taken as the systematic uncertainty.
- The prior distribution was simultaneously scaled by $(p_{\mathrm{T}}^{\mathrm{ch\,jet}})^{\pm 0.5}$ and a linear scaling in z_r by $\pm 50\%$ over its reported range. The average difference between the result unfolded with this prior and the original is taken as the systematic uncertainty.
- The detector-level binnings in z_r were varied to be finer and coarser than the nominal binning.
- The lower bound in the detector level charged-particle jet transverse momentum $p_{\mathrm{T,det}}^{\mathrm{ch\,jet}}$ range was varied by ± 5 GeV/c.

The total unfolding systematic uncertainty is then the standard deviation of the results from the variations, $\sqrt{\sum_{i=1}^{N} \sigma_i^2 / N}$, where $N = 4$ and σ_i is the systematic uncertainty due to a single variation, since they each comprise independent measurements of the same underlying systematic uncertainty in the regularization.

The constituent subtraction introduces a bias in the observed distributions, since it implicitly makes a

Table 1: Summary of systematic uncertainties on unfolded z_r distributions for $80 < p_{\mathrm{T}}^{\mathrm{ch\,jet}} < 120$ GeV/c. The ranges correspond to the minimum and maximum systematic uncertainties obtained.

	Relative uncertainty (%)				
pp	Trk. eff.	Unfolding	Generator		Total
$r = 0.1$	0–8%	1–6%	0–4%		2–10%
$r = 0.2$	0–10%	1–7%	0–3%		1–11%
Pb–Pb 0–10%	Trk. eff.	Unfolding	Generator	Bkgd. sub.	Total
$r = 0.1$	1–24%	3–17%	1–22%	5–10%	10–33%
$r = 0.2$	1–18%	1–10%	1–20%	1–6%	7–25%

choice of how much p_T to subtract from soft particles compared to the hard particles, and similarly for their angular distributions. To estimate the size of the systematic uncertainty related to the background subtraction, we varied R_{max} from "under-subtraction" ($R_{max} = 0.05$) to "over-subtraction" ($R_{max} = 0.7$), around the nominal value of $R_{max} = 0.25$. The maximum deviation of these two variations was assigned as the systematic uncertainty.

The systematic uncertainty due to the model-dependence of the generator used to construct the RM is estimated by comparing results obtained with PYTHIA8 [62] to those obtained with HERWIG7 [78] (in the pp case) or JEWEL 2.2.0 [79, 80] (in the Pb–Pb case). For HERWIG7, the default tune was used, and for JEWEL, we adopted the settings described in Ref. [81], with an initial temperature $T_i = 590$ MeV and no recoils. These RMs are then used to unfold the measured data, and the differences between PYTHIA8 and HERWIG7 (in the pp case) or PYTHIA8 and JEWEL (in the Pb–Pb case) are taken as a symmetric uncertainty.

5   Results

We report the z_r distributions for $r = 0.1$ and $r = 0.2$ in both pp and Pb–Pb collisions. All presented results use $R = 0.4$ jets reconstructed from charged particles at midrapidity, and are corrected for detector effects and (in Pb–Pb collisions) underlying-event fluctuations. We report results for $p_T^{ch\,jet}$ between 80 and 120 GeV/c in both pp and Pb–Pb collisions, as well as a result with finer binning in z_r for $p_T^{ch\,jet}$ between 100 and 150 GeV/c in Pb–Pb collisions. The distributions are reported as normalized differential cross sections,

$$\frac{1}{\sigma_{jet}}\frac{d\sigma}{dz_r} = \frac{1}{N_{jet}}\frac{dN}{dz_r},\tag{1}$$

where N_{jet} (σ_{jet}) is the number (cross section) of inclusive charged-particle jets within the given $p_T^{ch\,jet}$ interval, and N (σ) is the number (cross section) of subjets. With this normalization, the integral of Eq. (1) is equal to the average number of subjets per jet:

$$\left\langle N^{subjets} \right\rangle = \int_0^1 dz_r \frac{1}{\sigma_{jet}}\frac{d\sigma}{dz_r}.\tag{2}$$

Using the leading subjet distributions, we also compute the average "subjet energy loss":

$$\left\langle z_{loss} \right\rangle = 1 - \int_0^1 dz_r\, z_r \frac{1}{\sigma}\frac{d\sigma}{dz_r},\tag{3}$$

which describes the fraction of p_T inside the jet that is not contained within the leading subjet [47].

5.1   Subjet fragmentation in proton–proton collisions

Figures 2 and 3 show the measured z_r distributions in pp collisions at $\sqrt{s} = 5.02$ TeV for inclusive and leading subjets, respectively. For $z_r > 0.5$ the leading and inclusive subjet distributions are identical, as expected. In this region, the amplitude of the z_r distribution increases with z_r, with a more pronounced peak at large z_r for $r = 0.2$ than for $r = 0.1$ since larger subjets are more likely to capture a larger fraction of the jet energy. It is expected that as $z_r \to 1$, the distributions will eventually decrease due to the increased splitting probability of soft emissions [47]. This is, however, not visible in the data due to the coarseness of the bin sizes. As z_r becomes small, the inclusive subjet distribution grows due to soft radiations emitted from the leading subjet, whereas the leading subjet distribution falls to zero. The fraction of p_T inside the jet that is not contained within the leading subjet is $\langle z_{loss} \rangle = 0.21$ for $r = 0.1$ and decreases to $\langle z_{loss} \rangle = 0.10$ for $r = 0.2$.

The distributions are generally well described by PYTHIA8 [62,63], however some tension is observed in the largest z_r bin. This may be due to threshold logarithms of $1 - z$, which may contribute significantly at
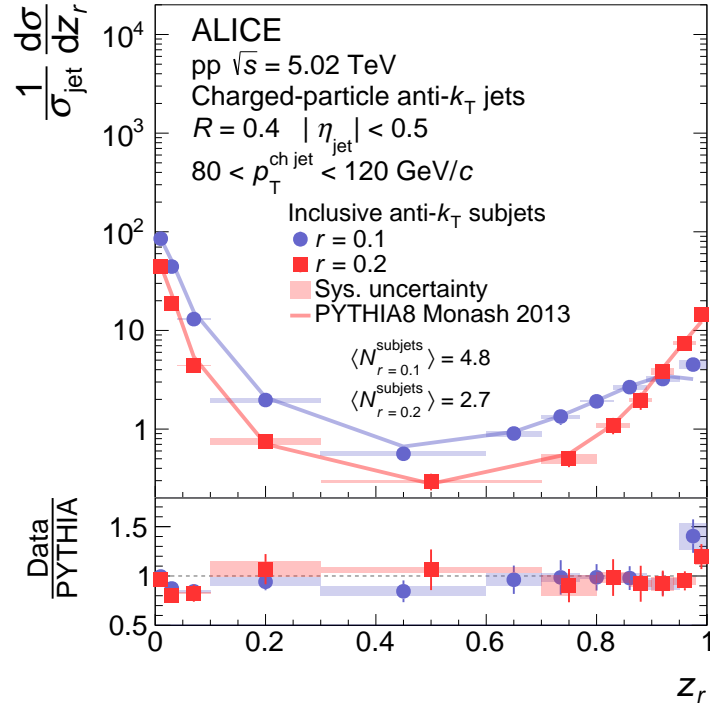
Figure 2: ALICE measurements of inclusive subjet z_r distribution in pp collisions for two different subjet radii, compared to PYTHIA8 [62, 63].
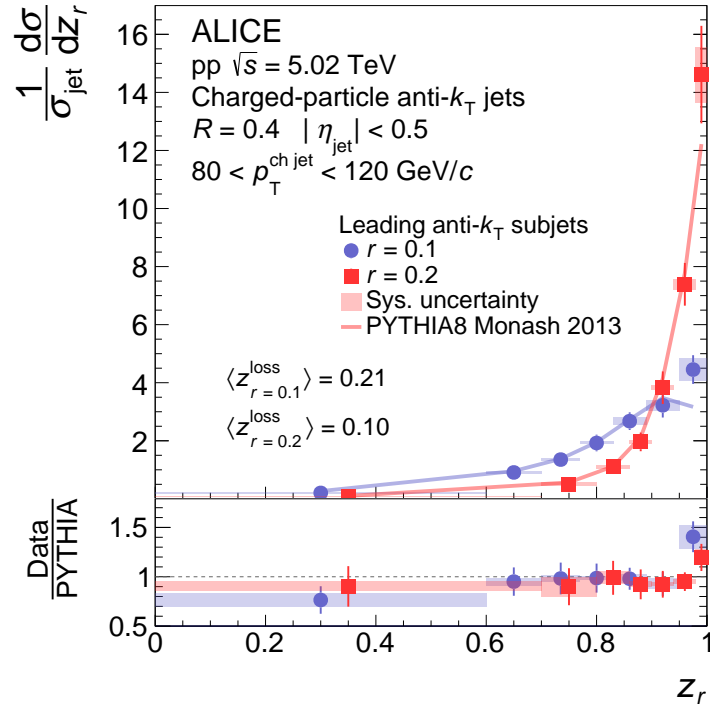
Figure 3: ALICE measurements of leading subjet z_r distribution in pp collisions for two different subjet radii, compared to PYTHIA8 [62, 63].

all orders in the strong coupling constant α_s and are not directly included in PYTHIA8 [47]. In addition, hadronization effects are expected to be significant at large z_r, since hadronization causes a smearing of the fragmentation across the boundary of the subjet and away from $z_r = 1$. However, due to ill-defined perturbative accuracy in general-purpose MC generators such as PYTHIA and the fact that they are tuned to reproduce data, it is difficult to draw detailed physics conclusions from their comparison to data. In order to study these effects in greater detail, we turn our attention to comparisons with analytical calculations based on perturbative QCD (pQCD).

Theoretical calculations of the z_r distribution in pp collisions have been carried out within the Soft-Collinear Effective Theory (SCET) framework [82] for both inclusive and leading subjets for a variety of r and R values [46, 47]. These calculations include all-order resummations of large logarithms of the jet radius and threshold logarithms to next-to-leading logarithmic (NLL$'$) accuracy. In order to compare these predictions to our measurement using charged-particle jets, a "forward folding" procedure based on MC event generators is applied to account for the fact that we measure only the charged component of jets [6]. Although the calculations are provided with hadronization corrections included [47], we additionally applied a bin-by-bin correction to account for multi-parton interactions using the procedure outlined in Ref. [6].
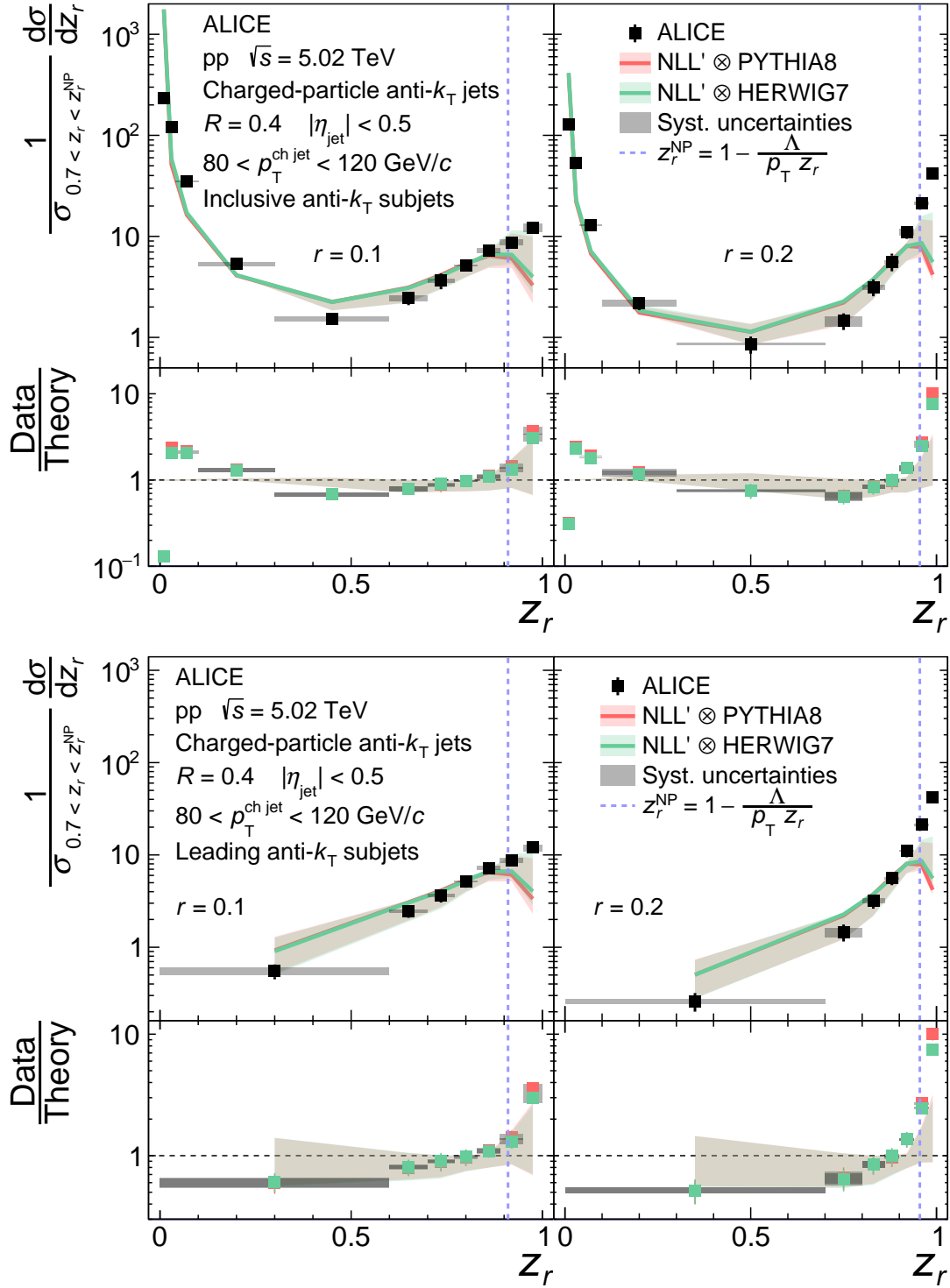
Figure 4 compares the measured z_r distributions to NLL$'$ calculations for inclusive and leading subjets [46, 47]. Two sets of NLL$'$ results are reported in the figure, which are obtained using either PYTHIA8 [62] or HERWIG7 [78] to account for charged-particle corrections, which show generally similar behavior. Uncertainties on the analytical predictions were estimated in Refs. [46, 47] by varying the combinations of scales that emerge in the calculation. The softest of these scales determines a transition between the perturbative and non-perturbative regimes:

$$z_r^{\mathrm{NP}} \approx 1 - \left(\frac{\Lambda}{p_{\mathrm{T}} r} \right), \tag{4}$$

where Λ is the energy scale at which α_s becomes non-perturbative. To denote this transition, we draw a dashed vertical blue line at $\Lambda = 1$ GeV/c, taking p_{T} to be the weighted average $p_{\mathrm{T}}^{\mathrm{ch\,jet}}$ in the considered interval scaled by 120% to approximately translate the p_{T} scale from charged-particle jets to full jets. While we draw the line at a discrete value in order to provide guidance, we remind the reader that the transition from values of z_r that are dominated by perturbative versus non-perturbative physics is actually smooth. Note that we display the non-perturbative transition only at large z_r, although a similar transition occurs at small z_r which is not addressed in this study [83, 84]. In the results shown in Fig 4, the cross section is scaled according to the integral of the distribution in a subset of the perturbative region,

$$\frac{1}{\sigma_{0.7 < z_r < z_r^{\mathrm{NP}}}} \frac{\mathrm{d}\sigma}{\mathrm{d}z_r}, \qquad \text{where} \qquad \sigma_{0.7 < z_r < z_r^{\mathrm{NP}}} = \int_{0.7}^{z_r^{\mathrm{NP}}} \frac{\mathrm{d}\sigma}{\mathrm{d}z_r} \mathrm{d}z_r. \tag{5}$$

In the inclusive subjet case, the measured z_r distributions are generally in agreement with the SCET calculations within uncertainties in the intermediate region $0.1 \lesssim z_r \lesssim 0.9$. The calculations begin to diverge from the data at large z_r in the non-perturbative regime, where the theoretical calculations are expected to break down. For $r = 0.1$, the calculations can, in fact, describe the data at large z_r within the systematic uncertainties of the calculation, whereas for $r = 0.2$ this is no longer the case. At small z_r, the calculations diverge from the data, with a large overestimate of the peak at $z_r < 0.02$ relative to the magnitude of the theoretical uncertainties. The calculations do not include a resummation of large logarithms of small z_r, which suggests that such a resummation is needed to describe the data. The measured distributions can serve to test future calculations that include small z_r resummation, which is relevant for attempts to calculate hadron observables using perturbatively calculable jet functions in the $r \to 0$ limit [83, 84].

9

Figure 4: ALICE measurements of inclusive (top) and leading (bottom) subjet z_r distributions in pp collisions at $\sqrt{s} = 5.02$ TeV, compared to NLL′ predictions carried out with SCET [46, 47] and corrected for missing neutral-particle energy and multi-parton interaction effects using PYTHIA8 [62] or HERWIG7 [78]. The shaded bands denote systematic uncertainty on the NLL′ calculations. The distributions are normalized such that the integral of the region defined by $0.7 < z_r < z_r^{NP}$ is unity, where z_r^{NP} is denoted by the dashed vertical blue lines. The non-perturbative scale in Eq. 4 is taken to be $\Lambda = 1$ GeV/c. In determining the normalization, bins that overlap with the dashed blue line are considered to be in the non-perturbative (right) region.

In the leading subjet case, we observe identical behavior to the inclusive subjet case in the region $z_r > 0.5$, since the distributions coincide. For $z_r < 0.5$, where the inclusive and leading distributions differ, the calculations involve nonlinear evolution of the jet fragmentation function. In this region, the NLL' results are consistent with the data within the uncertainties of the calculation. Note that this comparison involves only a single bin due to the fact that the z_r distributions fall steeply as z_r decreases. More differential data would allow for stricter tests of the non-linear evolution of leading jet fragmentation functions. A test of related calculations of leading dijet energy spectra have recently been examined in e^+e^- collisions [8], finding good agreement. Finally, we note that the quantity $\langle z_{\text{loss}} \rangle$ described in Eq. 3 is strongly affected by the non-perturbative region $z_r > z_r^{\text{NP}}$, since a significant fraction of the integral is located in this interval. This presents a challenge to the prospects for theoretically calculating $\langle z_{\text{loss}} \rangle$, and calls for further theoretical studies.

5.2 Subjet fragmentation in Pb–Pb collisions

Figures 5 and 6 show the leading subjet z_r distributions in pp and 0–10% central Pb–Pb collisions for $r = 0.1$ and $r = 0.2$, respectively, with their ratios displayed in the bottom panels. We report a restricted range in z_r in Pb–Pb collisions due to the contamination from the underlying event at low-z_r, as explained in Sec. 3, although we note that this excludes only a small portion of the leading subjet distribution. The reported distributions are accordingly normalized to the cross section of inclusive charged-particle jets conditioned with z_r in the reported range. The relative uncertainties are assumed to be uncorrelated between pp and Pb–Pb collisions, and are added in quadrature in the ratio.

For both $r = 0.1$ and $r = 0.2$, the distributions are consistent with no modification of the z_r distribution in central Pb–Pb compared to pp collisions. However, the distributions are also consistent with a hardening effect in Pb–Pb compared to pp collisions that reverses as $z_r \to 1$. For $r = 0.1$, we observe consistency with stronger hardening effects than for $r = 0.2$. To understand the behavior of the z_r distribution, we note that in vacuum there are significant differences in the parton-to-subjet fragmentation functions between quarks and gluons, with the fraction of quark-initiated jets increasing with z_r [47]. If the QGP suppresses gluon jets more than quark jets, then a hardening of the z_r distribution is expected – in line with previous measurements of hadron fragmentation [85]. On the other hand, medium-induced radiations will in general shift the distribution to smaller z_r. The competition between these two distinct sources of jet substructure modification – quark vs. gluon suppression and medium-induced radiation – can result in non-trivial modification to the shape of the z_r distribution in different intervals of z_r. As $z_r \to 1$, the jet sample in vacuum becomes almost entirely dominated by quark jets – thereby rendering the quark vs. gluon fraction modification negligible. This presents an opportunity to expose a region of quark-initiated jets depleted by soft medium-induced emissions. Our measurements are qualitatively consistent with such a modification pattern: a hardening of the z_r distribution due to the relative suppression of gluon vs. quark initiated jets, followed by a turnover of the distribution as $z_r \to 1$ due to medium-induced soft radiations.

We compare the ratio of the measurements in pp and Pb–Pb collisions with several theoretical models of jet quenching:

- *Medium jet functions* [46, 50] are a SCET-based calculation obtained by modifying the z_r distributions from pp collisions according to the medium-modified parton-to-jet fragmentation functions extracted in Ref. [50]. The quark/gluon fractions in the extracted medium-modified jet function exhibit a relative suppression factor of approximately four between gluon jets and quark jets.

- *JETSCAPE* [86] consists of a medium-modified parton shower calculated with the MATTER [88] model controlling the high-virtuality phase and the Linear Boltzmann Transport (LBT) model describing the low-virtuality phase [87]. The version of JETSCAPE used for this calculation employs a jet transport coefficient, $\hat{q}$, that includes dependence on parton virtuality, in addition to dependence on the local temperature and running of the parton-medium coupling. The calculation
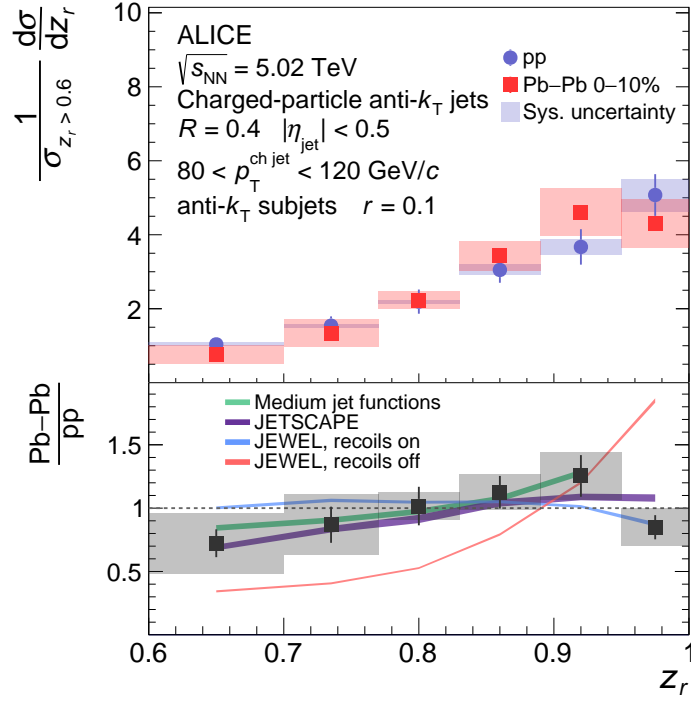
Figure 5: Measurements of subjet z_r distributions for subjet radius $r = 0.1$ in pp and 0–10% central Pb–Pb collisions. The bottom panel displays the ratio of the distributions in Pb–Pb to pp collisions, along with comparison to theoretical predictions [46, 50, 79, 80, 86–88].
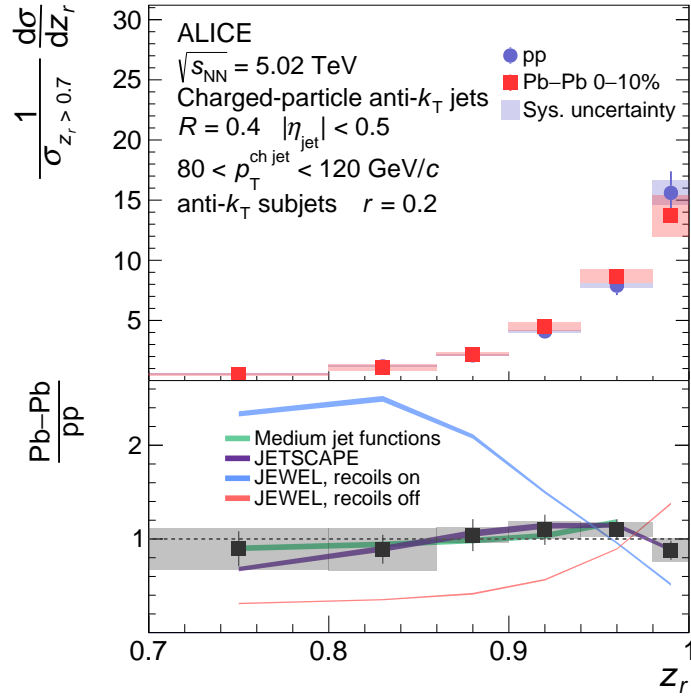
Figure 6: Measurements of subjet z_r distributions for subjet radius $r = 0.2$ in pp and 0–10% central Pb–Pb collisions. The bottom panel displays the ratio of the distributions in Pb–Pb to pp collisions, along with comparison to theoretical predictions [46, 50, 79, 80, 86–88].

includes medium recoil particles, and a subtraction of the thermal component of the recoils is performed by summing the transverse momentum of the thermal particles within the jet (subjet) radius and subtracting this from the corresponding jet (subjet) transverse momentum.

- *JEWEL* [79,80] implements BDMPS-based medium-induced gluon radiation in a medium modeled with a Bjorken expansion. We use JEWEL 2.2.0 with an initial temperature $T_i = 590$ MeV and initial quenching time $\tau_i = 0.4$, which provides an accurate description of a variety of jet quenching observables [81]. The impact of medium recoil is studied by displaying results both with and without recoils enabled. In the case with recoils included, the thermal component of the recoils is subtracted with the same method used in the JETSCAPE calculation (which is similar to the "4MomSub" method [81]) except randomly discarding 33% of the thermal particles (which JEWEL assigns to be neutral) in order to account for the fact that our measurement uses charged-particle jets.

For the JETSCAPE and JEWEL simulations, the width of the curves denotes statistical uncertainty. For the "Medium jet functions" calculation, systematic uncertainties are included but are smaller than the width of the plotted curve.

The comparison of our result to the "Medium jet functions" calculation provides a test of universality of jet fragmentation functions in the QGP, since the calculation uses a parton-to-jet function extracted from inclusive jet measurements, and employs it as the parton-to-subjet function in the z_r calculation. We find a consistent description of the z_r distribution, and therefore consistency with the universality of jet fragmentation in the QGP. While this does not exclude process-dependent effects or factorization breaking, it does place constraints on the magnitude of such effects, and establishes a new avenue to search for them. These measurements can be used to directly extract the parton-to-subjet function in future work and serve as input for global tests of factorization breaking in the QGP (see Ref. [50]).

The JETSCAPE model describes the data well within the precision of our measurement. The JEWEL model, on the other hand, describes the data well for $r = 0.1$ when recoils are included, but fails to describe the data for $r = 0.2$ or when recoils are not included. For both $r = 0.1$ and $r = 0.2$, there are large differences in the JEWEL predictions depending whether recoils are enabled, suggesting that this observable may be significantly impacted by medium response. In general, it is expected that medium response will soften the z_r distribution since it tends to broaden reconstructed jets. We indeed observe this in the results of the JEWEL calculations, where the z_r distribution in the largest z_r bin is significantly suppressed when recoils are included compared to when recoils are disabled. However, it appears that for $r = 0.2$, this suppression is significantly stronger than the experimental data allows (noting that the large enhancement observed at smaller z_r is necessitated by the suppression at large z_r due to the self-normalization condition). This corroborates previous observations that the medium response implementation in JEWEL, which does not include rescattering of the medium response particles, overestimates the impact of medium recoil, but that the calculations with and without recoil generally bracket the experimental data (see e.g. Ref. [32, 89]).

In order to test the r-dependence of the z_r distribution with higher precision, in Fig. 7 we compare the z_r distributions measured in 0–10% central Pb–Pb collisions with $r = 0.1$ and $r = 0.2$ for the $p_{\mathrm{T}}^{\mathrm{ch\,jet}}$ interval between 100 and 150 GeV/c. The ratio of the two distributions is shown in the bottom panel of Fig. 7. Since the two measurements are correlated, the systematic uncertainty of the ratio partially cancels out. While separate values of $\sigma_{z_r > 0.7}$ are used to normalize the $r = 0.1$ and $r = 0.2$ distributions, the normalization factors only differ by the integral of the $z_r < 0.7$ tails and are therefore within a few percent. We refrain from constructing the corresponding pp ratio due to sizeable statistical uncertainties of the recorded pp data set.

We compare the $\frac{r=0.1}{r=0.2}$ ratio to the JETSCAPE and JEWEL models discussed above. We find that JEWEL fails to describe the ratio either with recoils on or recoils off, but that the two implementations bracket
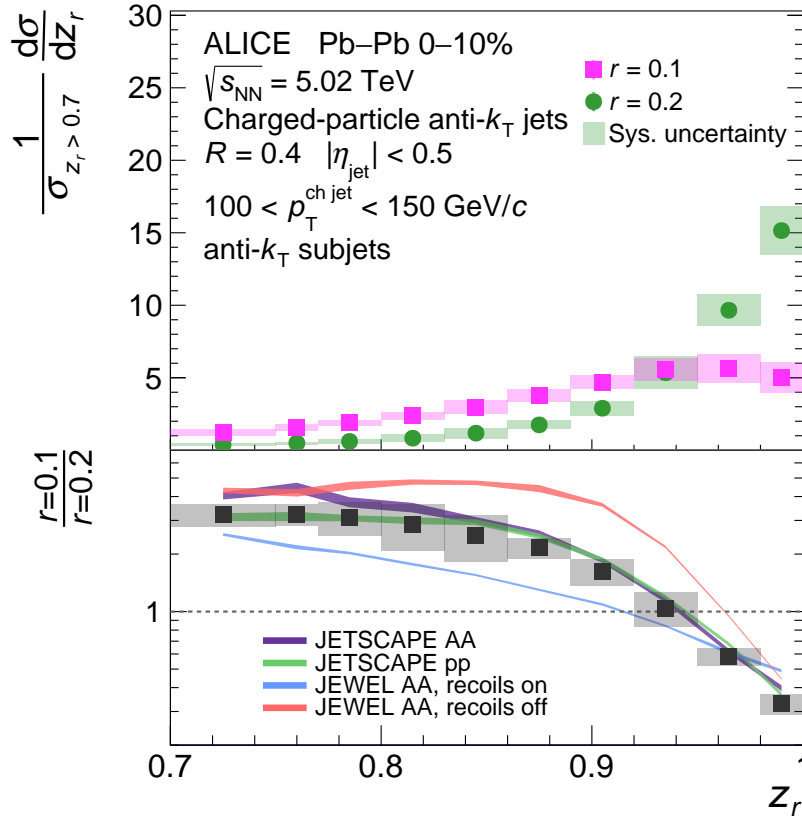
Figure 7: Measurements of subjet z_r distributions for subjet radii $r = 0.1$ and $r = 0.2$ in 0–10% central Pb–Pb collisions. The bottom panel displays the ratio of the distributions for $r = 0.1$ to $r = 0.2$, along with comparison to JEWEL and JETSCAPE model predictions [79, 80, 86–88].

most of the data. However, the JEWEL calculations predict that at large z_r, the $r = 0.1$ "core" of the jet contains more p_T relative to $r = 0.2$ as compared to the experimental data – i.e. that the large-z_r fragmentation is narrower in JEWEL than in experimental data.

The JETSCAPE model describes the ratio significantly better, however given the precision of the measurement, we find significant tension in the shape of the distribution with the JETSCAPE prediction. While this may not be immediately obvious by eye, we note that due to the self-normalization condition in the z_r distributions in the top panel of Fig. 7, a shift in one point necessitates an opposite shift in the remaining points to ensure the distribution integrates to unity. For example, if the value of the ratio in the rightmost bin $0.98 < z_r < 1$ of the JETSCAPE calculation were to move down, the leftmost bins near $0.7 < z_r < 0.8$ would have to compensate by moving up, rendering the calculation unable to reproduce the experimental data. The distribution from JETSCAPE simulations for pp collisions, on the other hand, describes the $\frac{r=0.1}{r=0.2}$ ratio well; however, one must use caution in interpreting this, since in Sec. 5.1 we have discussed challenges in achieving an accurate description of the pp baseline at large z_r. The JETSCAPE calculation exhibits a hint that the $r = 0.1$ "core" of the jet contains more p_T relative to $r = 0.2$ as compared to the experimental data, similar to JEWEL although with less significant tension.

6   Conclusions

We have presented new measurements of subjet fragmentation with ALICE. In pp collisions, we find agreement of pQCD calculations with the data in the perturbative regime at intermediate z_r and discrepancies at large z_r which may imply that threshold resummation and hadronization play important

roles as the distribution becomes increasingly non-perturbative. The PYTHIA8 event generator generally describes the data well, however some tension is observed at large z_r, which is consistent with these findings given that threshold resummation is not directly included in PYTHIA8. In the inclusive subjet case, we find a disagreement of the pQCD calculations with the data at small z_r, suggesting a need to include a small-z_r resummation in order to describe the data. These measurements provide future opportunities to study threshold and small-z_r resummations, and motivate new measurements extended to even smaller values of r, which are relevant for understanding parton-hadron duality and the interplay of jet observables and hadron observables as $r \to 0$ [83, 84].

In heavy-ion collisions, these measurements serve as a key ingredient to study the high-z region of jet quenching and test the universality of jet fragmentation in the QGP. By comparing the z_r distributions for $r = 0.1$ and $r = 0.2$ to Monte Carlo jet quenching models, we find indications that quenched jets at large z_r are narrower in JEWEL and JETSCAPE than in experimental data. By probing large z_r, these measurements can isolate a region of quark-dominated jets with an inclusive jet sample alone, offering the potential to expose a sample of jets depleted by medium-induced soft radiation. Together, our measurements demonstrate that while the large-z_r region is theoretically challenging to describe in pp collisions due to threshold resummation and hadronization effects, it is a particularly interesting region to study jet modification in heavy-ion collisions. This calls for theoretical investigation of the large-z_r region in greater detail. Future measurements of z_r in coincidence with other substructure observables such as the groomed jet radius [34] offer the potential to disentangle medium-induced soft radiation effects from differences in the suppression of gluon vs. quark jets. By comparing our measurements to perturbative calculations based on QCD factorization, we find consistency with the universality of jet fragmentation and no indication of factorization breaking in the QGP. These measurements can be used as input to extract the parton-to-subjet fragmentation function in future work and perform global tests of factorization breaking in the QGP.

References

[1] A. J. Larkoski, I. Moult, and B. Nachman, "Jet Substructure at the Large Hadron Collider: A Review of Recent Advances in Theory and Machine Learning", *Phys. Rept.* **841** (2020) 1–63, `arXiv:1709.04464 [hep-ph]`.

[2] R. Kogler *et al.*, "Jet Substructure at the Large Hadron Collider: Experimental Review", *Rev. Mod. Phys.* **91** (2019) 045003, `arXiv:1803.06991 [hep-ex]`.

[3] S. Marzani, G. Soyez, and M. Spannowsky, "Looking inside jets: an introduction to jet substructure and boosted-object phenomenology", *Lecture Notes in Physics* **958** (2019) , `arXiv:1901.10342 [hep-ph]`.

[4] **ATLAS** Collaboration, G. Aad *et al.*, "Measurement of soft-drop jet observables in pp collisions with the ATLAS detector at $\sqrt{s}$ =13 TeV", *Phys. Rev. D* **101** no. 5, (2020) 052007, `arXiv:1912.09837 [hep-ex]`.

[5] **CMS** Collaboration, A. M. Sirunyan *et al.*, "Measurement of jet substructure observables in $t\bar{t}$ events from proton-proton collisions at $\sqrt{s} = 13$TeV", *Phys. Rev. D* **98** no. 9, (2018) 092014, `arXiv:1808.07340 [hep-ex]`.

[6] **ALICE** Collaboration, "Measurements of the groomed and ungroomed jet angularities in pp collisions at $\sqrt{s} = 5.02$ TeV", `arXiv:2107.11303 [nucl-ex]`.

[7] **STAR** Collaboration, J. Adam *et al.*, "Measurement of groomed jet substructure observables in p+p collisions at $\sqrt{s}$ =200 GeV with STAR", *Phys. Lett. B* **811** (2020) 135846, `arXiv:2003.02114 [hep-ex]`.

[8] Y. Chen *et al.*, "Jet energy spectrum and substructure in e^+e^- collisions at 91.2 GeV with ALEPH Archived Data", `arXiv:2111.09914 [hep-ex]`.

 [9] **H1** Collaboration, V. Andreev *et al.*, "Measurement of lepton-jet correlation in deep-inelastic scattering with the H1 detector using machine learning for unfolding", `arXiv:2108.12376` `[hep-ex]`.

[10] J. D. Bjorken, "Highly Relativistic Nucleus-Nucleus Collisions: The Central Rapidity Region", *Phys. Rev. D* **27** (1983) 140–151.

[11] **STAR** Collaboration, J. Adams *et al.*, "Experimental and theoretical challenges in the search for the quark gluon plasma: The STAR Collaboration's critical assessment of the evidence from RHIC collisions", *Nucl. Phys. A* **757** (2005) 102–183, `arXiv:nucl-ex/0501009`.

[12] **PHENIX** Collaboration, K. Adcox *et al.*, "Formation of dense partonic matter in relativistic nucleus-nucleus collisions at RHIC: Experimental evaluation by the PHENIX collaboration", *Nucl. Phys. A* **757** (2005) 184–283, `arXiv:nucl-ex/0410003`.

[13] B. Muller, J. Schukraft, and B. Wyslouch, "First Results from Pb+Pb collisions at the LHC", *Ann. Rev. Nucl. Part. Sci.* **62** (2012) 361–386, `arXiv:1202.3233` `[hep-ex]`.

[14] P. Braun-Munzinger, V. Koch, T. Schäfer, and J. Stachel, "Properties of hot and dense matter from relativistic heavy ion collisions", *Phys. Rept.* **621** (2016) 76–126, `arXiv:1510.00442` `[nucl-th]`.

[15] W. Busza, K. Rajagopal, and W. van der Schee, "Heavy Ion Collisions: The Big Picture, and the Big Questions", *Ann. Rev. Nucl. Part. Sci.* **68** (2018) 339–376, `arXiv:1802.04801` `[hep-ph]`.

[16] J. E. Bernhard, J. S. Moreland, and S. A. Bass, "Bayesian estimation of the specific shear and bulk viscosity of quark–gluon plasma", *Nature Phys.* **15** no. 11, (2019) 1113–1117.

[17] J. E. Parkkila, A. Onnerstad, and D. J. Kim, "Bayesian estimation of the specific shear and bulk viscosity of the quark-gluon plasma with additional flow harmonic observables", `arXiv:2106.05019` `[hep-ph]`.

[18] G. Nijs, W. van der Schee, U. Gürsoy, and R. Snellings, "Transverse Momentum Differential Global Analysis of Heavy-Ion Collisions", *Phys. Rev. Lett.* **126** no. 20, (2021) 202301, `arXiv:2010.15130` `[nucl-th]`.

[19] **JETSCAPE** Collaboration, D. Everett *et al.*, "Multisystem Bayesian constraints on the transport coefficients of QCD matter", *Phys. Rev. C* **103** no. 5, (2021) 054904, `arXiv:2011.01430` `[hep-ph]`.

[20] S. Y. F. Liu and R. Rapp, "Spectral and transport properties of quark–gluon plasma in a nonperturbative approach", *Eur. Phys. J. A* **56** no. 2, (2020) 44, `arXiv:1612.09138` `[nucl-th]`.

[21] F. Scardina, S. K. Das, V. Minissale, S. Plumari, and V. Greco, "Estimating the charm quark diffusion coefficient and thermalization time from D meson spectra at energies available at the BNL Relativistic Heavy Ion Collider and the CERN Large Hadron Collider", *Phys. Rev. C* **96** no. 4, (2017) 044905, `arXiv:1707.05452` `[nucl-th]`.

[22] Y. Xu, J. E. Bernhard, S. A. Bass, M. Nahrgang, and S. Cao, "Data-driven analysis for the temperature and momentum dependence of the heavy-quark diffusion coefficient in relativistic heavy-ion collisions", *Phys. Rev. C* **97** no. 1, (2018) 014907, `arXiv:1710.00807` `[nucl-th]`.

[23] **JET** Collaboration, K. M. Burke *et al.*, "Extracting the jet transport coefficient from jet quenching in high-energy heavy-ion collisions", *Phys. Rev. C* **90** no. 1, (2014) 014909, `arXiv:1312.5003` `[nucl-th]`.

[24] C. Andrés, N. Armesto, M. Luzum, C. A. Salgado, and P. Zurita, "Energy versus centrality dependence of the jet quenching parameter $\hat{q}$ at RHIC and LHC: a new puzzle?", *Eur. Phys. J. C* **76** no. 9, (2016) 475, `arXiv:1606.04837` `[hep-ph]`.

[25] M. Xie, S.-Y. Wei, G.-Y. Qin, and H.-Z. Zhang, "Extracting jet transport coefficient via single hadron and dihadron productions in high-energy heavy-ion collisions", *Eur. Phys. J. C* **79** no. 7, (2019) 589, `arXiv:1901.04155` `[hep-ph]`.

[26] **JETSCAPE** Collaboration, S. Cao *et al.*, "Determining the jet transport coefficient from inclusive hadron suppression measurements using Bayesian parameter estimation", *Phys. Rev. C* **104** no. 2, (2021) 024905, arXiv:2102.11337 [nucl-th].

[27] G.-Y. Qin and X.-N. Wang, "Jet quenching in high-energy heavy-ion collisions", *Int. J. Mod. Phys. E* **24** no. 11, (2015) 1530014, arXiv:1511.00790 [hep-ph].

[28] J.-P. Blaizot and Y. Mehtar-Tani, "Jet Structure in Heavy Ion Collisions", *Int. J. Mod. Phys. E* **24** no. 11, (2015) 1530012, arXiv:1503.05958 [hep-ph].

[29] A. Majumder and M. Van Leeuwen, "The Theory and Phenomenology of Perturbative QCD Based Jet Quenching", *Prog. Part. Nucl. Phys.* **66** (2011) 41–92, arXiv:1002.2206 [hep-ph].

[30] **ALICE** Collaboration, S. Acharya *et al.*, "Measurements of inclusive jet spectra in pp and central Pb–Pb collisions at $\sqrt{s_{\mathrm{NN}}} = 5.02$ TeV", *Phys. Rev. C* **101** no. 3, (2020) 034911, arXiv:1909.09718 [nucl-ex].

[31] **ATLAS** Collaboration, M. Aaboud *et al.*, "Measurement of the nuclear modification factor for inclusive jets in Pb+Pb collisions at $\sqrt{s_{\mathrm{NN}}} = 5.02$ TeV with the ATLAS detector", *Phys. Lett. B* **790** (2019) 108–128, arXiv:1805.05635 [nucl-ex].

[32] **CMS** Collaboration, A. M. Sirunyan *et al.*, "First measurement of large area jet transverse momentum spectra in heavy-ion collisions", *JHEP* **05** (2021) 284, arXiv:2102.13080 [hep-ex].

[33] **STAR** Collaboration, J. Adam *et al.*, "Measurement of inclusive charged-particle jet production in Au + Au collisions at $\sqrt{s_{NN}} = 200$ GeV", *Phys. Rev. C* **102** no. 5, (2020) 054913, arXiv:2006.00582 [nucl-ex].

[34] **ALICE** Collaboration, S. Acharya *et al.*, "Measurement of the groomed jet radius and momentum splitting fraction in pp and Pb−Pb collisions at $\sqrt{s_{\mathrm{NN}}} = 5.02$ TeV", *Phys. Rev. Lett.* **128** no. 10, (2022) 102001, arXiv:2107.12984 [nucl-ex].

[35] **ALICE** Collaboration, S. Acharya *et al.*, "Medium modification of the shape of small-radius jets in central Pb-Pb collisions at $\sqrt{s_{\mathrm{NN}}} = 2.76$ TeV", *JHEP* **10** (2018) 139, arXiv:1807.06854 [nucl-ex].

[36] **ATLAS** Collaboration, M. Aaboud *et al.*, "Measurement of jet fragmentation in Pb+Pb and *pp* collisions at $\sqrt{s_{NN}} = 5.02$ TeV with the ATLAS detector", *Phys. Rev. C* **98** no. 2, (2018) 024908, arXiv:1805.05424 [nucl-ex].

[37] **ATLAS** Collaboration, M. Aaboud *et al.*, "Comparison of Fragmentation Functions for Jets Dominated by Light Quarks and Gluons from *pp* and Pb+Pb Collisions in ATLAS", *Phys. Rev. Lett.* **123** no. 4, (2019) 042001, arXiv:1902.10007 [nucl-ex].

[38] **CMS** Collaboration, S. Chatrchyan *et al.*, "Measurement of Jet Fragmentation in PbPb and pp Collisions at $\sqrt{s_{NN}} = 2.76$ TeV", *Phys. Rev. C* **90** no. 2, (2014) 024908, arXiv:1406.0932 [nucl-ex].

[39] **CMS** Collaboration, A. M. Sirunyan *et al.*, "Observation of Medium-Induced Modifications of Jet Fragmentation in Pb-Pb Collisions at $\sqrt{s_{NN}} = 5.02$ TeV Using Isolated Photon-Tagged Jets", *Phys. Rev. Lett.* **121** no. 24, (2018) 242301, arXiv:1801.04895 [hep-ex].

[40] **CMS** Collaboration, A. M. Sirunyan *et al.*, "Measurement of the Splitting Function in *pp* and Pb-Pb Collisions at $\sqrt{s_{\mathrm{NN}}} = 5.02$ TeV", *Phys. Rev. Lett.* **120** no. 14, (2018) 142302, arXiv:1708.09429 [nucl-ex].

[41] **CMS** Collaboration, A. M. Sirunyan *et al.*, "Measurement of the groomed jet mass in PbPb and pp collisions at $\sqrt{s_{\mathrm{NN}}} = 5.02$ TeV", *JHEP* **10** (2018) 161, arXiv:1805.05145 [hep-ex].

[42] **ALICE** Collaboration, J. Adam *et al.*, "Measurement of jet quenching with semi-inclusive hadron-jet distributions in central Pb-Pb collisions at $\sqrt{s_{\mathrm{NN}}} = 2.76$ TeV", *JHEP* **09** (2015) 170, arXiv:1506.03984 [nucl-ex].

[43] **STAR** Collaboration, L. Adamczyk *et al.*, "Measurements of jet quenching with semi-inclusive hadron+jet distributions in Au+Au collisions at $\sqrt{s_{NN}}$ = 200 GeV", *Phys. Rev. C* **96** no. 2, (2017) 024905, `arXiv:1702.01108 [nucl-ex]`.

[44] M. Cacciari, G. P. Salam, and G. Soyez, "The anti-k_t jet clustering algorithm", *JHEP* **04** (2008) 063, `arXiv:0802.1189 [hep-ph]`.

[45] L. Dai, C. Kim, and A. K. Leibovich, "Fragmentation of a Jet with Small Radius", *Phys. Rev. D* **94** no. 11, (2016) 114023, `arXiv:1606.07411 [hep-ph]`.

[46] Z.-B. Kang, F. Ringer, and W. J. Waalewijn, "The Energy Distribution of Subjets and the Jet Shape", *JHEP* **07** (2017) 064, `arXiv:1705.05375 [hep-ph]`.

[47] D. Neill, F. Ringer, and N. Sato, "Leading jets and energy loss", *JHEP* **07** (2021) 041, `arXiv:2103.16573 [hep-ph]`.

[48] L. Apolinário, J. G. Milhano, M. Ploskon, and X. Zhang, "Novel subjet observables for jet quenching in heavy-ion collisions", *Eur. Phys. J. C* **78** no. 6, (2018) 529, `arXiv:1710.07607 [hep-ph]`.

[49] P. Caucal, E. Iancu, A. H. Mueller, and G. Soyez, "Nuclear modification factors for jet fragmentation", *JHEP* **10** (2020) 204, `arXiv:2005.05852 [hep-ph]`.

[50] J.-W. Qiu, F. Ringer, N. Sato, and P. Zurita, "Factorization of jet cross sections in heavy-ion collisions", *Phys. Rev. Lett.* **122** no. 25, (2019) 252301, `arXiv:1903.01993 [hep-ph]`.

[51] **ALICE** Collaboration, K. Aamodt *et al.*, "The ALICE experiment at the CERN LHC", *JINST* **3** (2008) S08002.

[52] **ALICE** Collaboration, B. Abelev *et al.*, "Performance of the ALICE Experiment at the CERN LHC", *Int. J. Mod. Phys. A* **29** (2014) 1430044, `arXiv:1402.4476 [nucl-ex]`.

[53] **ALICE** Collaboration, E. Abbas *et al.*, "Performance of the ALICE VZERO system", *JINST* **8** (2013) P10016, `arXiv:1306.3130 [nucl-ex]`.

[54] **ALICE** Collaboration, B. Abelev *et al.*, "Centrality determination of Pb-Pb collisions at $\sqrt{s_{NN}}$ = 2.76 TeV with ALICE", *Phys. Rev. C* **88** no. 4, (2013) 044909, `arXiv:1301.4361 [nucl-ex]`.

[55] **ALICE** Collaboration, S. Acharya *et al.*, "Centrality determination in heavy-ion collisions", *ALICE-PUBLIC-2018-011* . `https://cds.cern.ch/record/2636623`.

[56] **ALICE** Collaboration, S. Acharya *et al.*, "ALICE 2017 luminosity determination for pp collisions at $\sqrt{s}$ =5 TeV", *ALICE-PUBLIC-2018-014* . `http://cds.cern.ch/record/2648933`.

[57] J. Alme and et al., "The ALICE TPC, a large 3-dimensional tracking device with fast readout for ultra-high multiplicity events", *Nucl. Instrum. Meth. Phys. Res. A* **622** (2010) 316–367.

[58] **ALICE** Collaboration, "Alignment of the ALICE Inner Tracking System with cosmic-ray tracks", *JINST* **5** (2010) P03003.

[59] H.-M. Chang, M. Procura, J. Thaler, and W. J. Waalewijn, "Calculating Track-Based Observables for the LHC", *Phys. Rev. Lett.* **111** (2013) 102002, `arXiv:1303.6637 [hep-ph]`.

[60] H. Chen, I. Moult, X. Zhang, and H. X. Zhu, "Rethinking jets with energy correlators: Tracks, resummation, and analytic continuation", *Phys. Rev. D* **102** (2020) 054012, `arXiv:2004.11381 [hep-ph]`.

[61] Y.-T. Chien, R. Rahn, S. Schrijnder van Velzen, D. Y. Shao, W. J. Waalewijn, and B. Wu, "Recoil-free azimuthal angle for precision boson-jet correlation", *Phys. Lett. B* **815** (2021) 136124, `arXiv:2005.12279 [hep-ph]`.

[62] T. Sjöstrand, S. Ask, J. R. Christiansen, R. Corke, N. Desai, P. Ilten, S. Mrenna, S. Prestel, C. O. Rasmussen, and P. Z. Skands, "An introduction to PYTHIA 8.2", *Comput. Phys. Commun.* **191** (2015) 159–177, `arXiv:1410.3012 [hep-ph]`.

[63] P. Skands, S. Carrazza, and J. Rojo, "Tuning PYTHIA 8.1: the Monash 2013 Tune", *Eur. Phys. J. C* **74** (2014) 3024, `arXiv:1404.5630 [hep-ph]`.

[64] R. Brun, F. Bruyant, M. Maire, A. C. McPherson, and P. Zanarini, *GEANT 3: user's guide Geant 3.10, Geant 3.11; rev. version.* CERN, Geneva, 1987. `https://cds.cern.ch/record/1119728`.

[65] M. Gyulassy and X.-N. Wang, "HIJING 1.0: A Monte Carlo program for parton and particle production in high-energy hadronic and nuclear collisions", *Comput. Phys. Commun.* **83** (1994) 307, `arXiv:nucl-th/9502021`.

[66] M. Cacciari, G. P. Salam, and G. Soyez, "FastJet User Manual", *Eur. Phys. J. C* **72** (2012) 1896, `arXiv:1111.6097 [hep-ph]`.

[67] M. Cacciari, G. P. Salam, and G. Soyez, "The Catchment Area of Jets", *JHEP* **04** (2008) 005, `arXiv:0802.1188 [hep-ph]`.

[68] **ALICE** Collaboration, B. Abelev *et al.*, "Measurement of Event Background Fluctuations for Charged Particle Jet Reconstruction in Pb-Pb collisions at $\sqrt{s_{NN}} = 2.76$ TeV", *JHEP* **03** (2012) 053, `arXiv:1201.2423 [hep-ex]`.

[69] P. Berta, M. Spousta, D. W. Miller, and R. Leitner, "Particle-level pileup subtraction for jets and jet shapes", *JHEP* **06** (2014) 092, `arXiv:1403.3108 [hep-ex]`.

[70] P. Berta, L. Masetti, D. W. Miller, and M. Spousta, "Pileup and Underlying Event Mitigation with Iterative Constituent Subtraction", *JHEP* **08** (2019) 175, `arXiv:1905.03470 [hep-ph]`.

[71] **ALICE** Collaboration, S. Acharya *et al.*, "The ALICE definition of primary particles", *ALICE-PUBLIC-2017-005* . `https://cds.cern.ch/record/2270008`.

[72] **ALICE** Collaboration, B. Abelev *et al.*, "Measurement of charged jet suppression in Pb-Pb collisions at $\sqrt{s_{NN}} = 2.76$ TeV", *JHEP* **03** (2014) 013, `arXiv:1311.0633 [nucl-ex]`.

[73] J. Mulligan and M. Ploskon, "Identifying groomed jet splittings in heavy-ion collisions", *Phys. Rev. C* **102** no. 4, (2020) 044913, `arXiv:2006.01812 [hep-ph]`.

[74] **STAR** Collaboration, M. S. Abdallah *et al.*, "Differential measurements of jet substructure and partonic energy loss in Au+Au collisions at $\sqrt{S_{NN}} =200$ GeV", `arXiv:2109.09793 [nucl-ex]`.

[75] G. D'Agostini, "Improved iterative Bayesian unfolding", `arXiv:1010.0632 [physics.data-an]`.

[76] G. D'Agostini, "A multidimensional unfolding method based on bayes' theorem", *Nucl. Instrum. Meth. Phys. Res. A* **362** (1995) 487–498.

[77] "RooUnfold." `http://hepunx.rl.ac.uk/~adye/software/unfold/RooUnfold.html`.

[78] J. Bellm *et al.*, "Herwig 7.0/Herwig++ 3.0 release note", *Eur. Phys. J. C* **76** (2016) 196, `arXiv:1512.01178 [hep-ph]`.

[79] K. C. Zapp, F. Krauss, and U. A. Wiedemann, "A perturbative framework for jet quenching", *J. High Energ. Phys.* **03** (2013) 080, `arXiv:1212.1599 [hep-ph]`.

[80] K. C. Zapp, "JEWEL 2.0.0: directions for use", *Eur. Phys. J. C* **74** (2014) 2762, `arXiv:1311.0048 [hep-ph]`.

[81] R. Kunnawalkam Elayavalli and K. C. Zapp, "Medium response in JEWEL and its impact on jet shape observables in heavy ion collisions", *J. High Energ. Phys.* **07** (2017) 141, `arXiv:1707.01539 [hep-ph]`.

[82] C. W. Bauer, D. Pirjol, and I. W. Stewart, "Soft collinear factorization in effective field theory", *Phys. Rev. D* **65** (Feb, 2002) 054022, `arXiv:hep-ph/0109045`.

[83] D. Neill and F. Ringer, "Soft Fragmentation on the Celestial Sphere", *JHEP* **06** (2020) 086, `arXiv:2003.02275 [hep-ph]`.

[84] D. Neill, "The Fragmentation Spectrum from Space-Time Reciprocity", *JHEP* **03** (2021) 081, `arXiv:2010.02934 [hep-ph]`.

[85] M. Spousta and B. Cole, "Interpreting single jet measurements in Pb + Pb collisions at the LHC", *Eur. Phys. J. C* **76** no. 2, (2016) 50, `arXiv:1504.05169 [hep-ph]`.

[86] J. H. Putschke *et al.*, "The JETSCAPE framework", `arXiv:1903.07706 [nucl-th]`.

[87] Y. He, T. Luo, X.-N. Wang, and Y. Zhu, "Linear Boltzmann Transport for Jet Propagation in the Quark-Gluon Plasma: Elastic Processes and Medium Recoil", *Phys. Rev. C* **91** (2015) 054908, `arXiv:1503.03313 [nucl-th]`. [Erratum: Phys.Rev.C 97, 019902 (2018)].

[88] A. Majumder, "Incorporating Space-Time Within Medium-Modified Jet Event Generators", *Phys. Rev. C* **88** (2013) 014909, `arXiv:1301.5323 [nucl-th]`.

[89] **ALICE** Collaboration, "First measurement of jet mass in Pb–Pb and p–Pb collisions at the LHC", *Phys. Lett. B* **776** (2018) 249–264, `arXiv:1702.00804 [nucl-ex]`.